JOURNAL OF CHEMICAL PHYSICS VOLUME 117, NUMBER 19 15 NOVEMBER 2002

Two-photon photodissociation of NO through Rydberg levels in the 265–278 nm region: Spectra and photofragment angular distributions

B. R. Cosofret, H. M. Lambert, and P. L. Houston
Department of Chemistry and Chemical Biology, Cornell University, Ithaca, New York 14853-1301

(Received 17 June 2002; accepted 20 August 2002)

The spectroscopy and dynamics of the NO photodissociation through Rydberg levels near 74 000 cm^{-1} have been investigated following two-photon excitation. The $6d\pi^-(v=1)$ and $5s\sigma(v=3)$ levels overlap near 74 070 cm^{-1}. Assignment of the rotational transitions for these levels has been aided by the use of the photoproduct angular distributions measured using product imaging techniques. Product imaging was also used to investigate the $8d\pi^-(v=1)$ and $5s\sigma(v=2)$ regions assigned by previous investigators. In all cases, the major products were $\mathrm{N}(^2D)+\mathrm{O}(^3P)$. The angular distributions vary strongly with rotational transition and with the assumed intermediate in the two-photon excitation scheme and can, for the most part, be predicted by calculation. They demonstrate that, for the Rydberg levels examined, the major contribution to the two-photon line strength is a Π intermediate, likely the $C\,^2\Pi$ state, with less than a 30% amplitude contribution from either a Σ or Δ intermediate. © *2002 American Institute of Physics.* [DOI: 10.1063/1.1513458]

I. INTRODUCTION

The spectroscopy of NO Rydberg levels has been a subject of continuing interest for over 50 years. The low ionization potential of NO (9.25 eV), makes the Rydberg levels accessible by one-photon excitation at vacuum ultraviolet (VUV) wavelengths around 130 nm. The detailed absorption spectra recorded with the high resolution spectrographs at the National Research Council in Ottawa have been published in atlas form.[1] A review of the early work was published in 1976.[2] More recently, NO Rydberg levels have been accessed by multiphoton laser excitation techniques, which conveniently allow the use of longer wavelength radiation and result in excitation to Rydberg levels not accessible by a one-photon transition.[3–18] The optical selection rule for the change in the atomiclike orbital angular momentum of the Rydberg electron is $\Delta\ell=\pm1$ for each photon absorbed in the transition. As a result, the *d*-like character of the highest occupied molecular orbital for ground state NO should result in enhanced excitation to *p* and *f* Rydberg states for a one-photon transition, whereas a two-photon transition should enhance the excitation of *s*, *d* or *g* Rydberg levels. In addition to these general guidelines, the nature of the intermediate state(s) and the presence of predissociation of the excited Rydberg levels also affects the spectrum.

Although it is possible to make a multiphoton process resonant with a known intermediate state by judicious choice of excitation wavelength, in general, there will be more than one intermediate state, either real or virtual, that will lead to the same final state. A complete understanding of the multiphoton process requires knowledge of the relative contributions of the intermediate states. Few ways to gain this knowledge are available. The absence of two-photon lines at low *J* for certain branches or the differing line intensities and branches can provide information on the symmetry of the intermediate state. As an example, the absence of an entire branch has been observed in several studies and is attributed to parity selectivity in multiphoton $\Pi\leftarrow\Pi$ excitation through Σ intermediates.[17,18] In principle, rotational line strength expressions derived for multiphoton excitation of diatomic molecules[17–20] may be explicitly summed over all intermediate states, weighted by the transition moment and an energy mismatch denominator, but in practice, sufficiently detailed information about the relative transition moments is lacking. Thus, the determination of the proportionate contribution to the spectrum from each multiphoton pathway is not routine.

Another factor that may affect the observed molecular two-photon spectrum is predissociation from Rydberg levels at energies above the several dissociation limits to atomic products. Pratt *et al.*[18] investigated the two-photon excitation to the $nd\pi$ Rydberg levels of NO for $n=5,7-12$ and demonstrated that the spectra obtained were consistent with a $^2\Pi(b)\leftarrow{}^2\Lambda(b)\leftarrow{}^2\Pi(a)$ excitation scheme with $\Lambda=\Sigma,\ \Pi$ estimated to be a 1:1 mixture for the intermediate states, and in which only transitions to the Π^- component of the upper state appeared. They surmised that the absence of the Π^+ component was due to a fast predissociation process from these levels. Clearly a combined strategy of detecting parent and dissociation products as a function of excitation wavelength would be helpful in elucidating the dynamics of the Rydberg levels in this region. The current study pursues this strategy. We will show, further, that the angular distribution of the dissociation products can provide information about the intermediate state in the two-photon excitation. These new tools are illustrated by further work on the spectra of NO Rydberg levels.

The NO spectral region accessed by two photons at wavelengths near 269 nm has been of interest since Slanger's group developed the $(2+1)$ resonance enhanced multiphoton ionization (REMPI) scheme to detect $\mathrm{N}(^2D)$ and showed that NO was a good source of $\mathrm{N}(^2D)$ at these wavelengths.[21,22] They observed that the total ion yield increased dramatically in a two laser pump and probe experiment when the photolysis laser was tuned across the rotational structure of a nearby Rydberg state and the probe laser was fixed on the N(^2D) REMPI transition. Based on unpublished spectra obtained from Miescher and Dressler, the rotational spectrum was identified as the $S\,^2\Sigma^+ \leftarrow X\,^2\Pi$ (3,0) band, which corresponds to excitation to a $5s\sigma$ Rydberg level.

Further work in a similar pump–probe experiment in this spectral region was carried out by Umemoto and Matsumoto,[23] who employed time of flight mass resolution to distinguish between NO$^+$ and N$^+$, higher resolution laser bandwidth, lower pressures, and partial cooling provided by an effusive jet. These workers assigned the spectrum to be a blend of the $5s\sigma \leftarrow X(3,0)$ band and the $6d\pi^- \leftarrow X(1,0)$ band. The latter additional assignment was based on work by Pratt *et al.*,[18] who noted that the spectrum was a blend of transitions to these two Rydberg levels, $5s\sigma(v=3)$ and $6d\pi^-(v=1)$ but did not attempt to analyze the spectrum.

Only recently has attention been given to the angular distribution of the products of NO predissociation from Rydberg states.[21–24] Bakker *et al.* have investigated two-photon dissociation of NO using the technique of velocity map imaging of the product O($^3P_2$) both using sequential two color excitation through the $A(^2\Sigma^+)$ state and one color, two-photon excitation near 275 nm.[25,26] In addition to information about the branching between product channels O(^3P) $+$N(^4S) and O(^3P)$+$N(^2D), the images provided evidence that the angular distributions taken across the $4d\pi^- \leftarrow X(2,0)$ band and the $5d\pi^- \leftarrow X(1,0)$ band varied significantly, despite the apparently poor rotational resolution.

In this work, we have used two-photon excitation to populate the $8d\pi^-(v=1)$, the $6d\pi^-(v=1)/5s\sigma(v=3)$, and the $5s\sigma(v=2)$ Rydberg levels in jet-cooled NO at wavelengths near 265 nm, 270 and 278 nm, respectively. Velocity mapped images of the dissociation product O($^3P_2$) were recorded at various rotational lines in these regions, and the resulting angular distributions were compared to quantum mechanical theoretical calculations. Not only did the angular distributions aid in confirming spectral assignments but they also distinguished between Σ, Π, and Δ intermediate states.

II. EXPERIMENT

The technique of ion imaging has been described in more detail elsewhere.[27,28] A 10% NO/He (Matheson) gas mixture was used from the cylinder without further purification. The gas was expanded at 17 psia through a 0.5 mm diam pulsed nozzle and collimated by a 0.5 mm diam skimmer mounted 1.0 cm away from the nozzle orifice. Further downstream, the molecular beam was crossed at right angles by two counterpropagating laser beams, one used to dissociate the molecules and the other to probe the resulting fragments. The O($^3P_2$) and N($^2D_{5/2}$) fragments were probed using $(2+1)$ REMPI schemes at 225.65 nm and 269 nm, respectively.[9,29–31] Due to the large Doppler widths it was necessary to scan the probe laser over the resonances to ensure that all product atom velocities were detected with equal sensitivity.

The dissociation laser radiation between 265 and 279 nm was produced by a Nd:YAG pumped SCANMATE dye laser (Lambda Physik) with Coumarin 540 A dye using second harmonic generation with typical powers of 0.5–1.0 mJ/pulse. The output from a second Nd:YAG pumped dye laser (Spectra Physics PDL pumped by Spectra Physics GCR230) was frequency doubled and mixed with the Nd:YAG fundamental using a WEX box in order to produce the 225.65 nm probe light with typical powers of 0.5 mJ/pulse. The photolysis and the probe beams were focused in the interaction region by two 25 cm focal length plano-convex lenses. The dissociation and ionization laser polarizations were parallel to the plane of the detector. Additional data were also taken with the ionization laser polarization perpendicular to the plane of the detector, while maintaining the photolysis vector parallel to the face of the detector. A delay time between the pump and probe lasers of 10 ns was typically used.

The imaging technique uses an electrostatic immersion lens which serves to extract the ionized N($^2D_{5/2}$) or O($^3P_2$) fragments from the interaction region and to focus ions with equal velocity vectors to the same point on the detector.[32] The ions were imaged by a position sensitive detector consisting of a chevron-mounted, double microchannel plate (MCP) assembly (Galileo) coupled to a fast phosphor screen. The image on the screen was recorded by a 640×480 pixel CCD camera (Xybion). Both the MCP and the camera were electronically gated to collect signal corresponding to only the mass of either the N($^2D_{5/2}$) fragment or the O($^3P_2$) fragment. Signal levels were kept below 100 ions per frame to ensure accurate ion counting. Data were accumulated typically for 45 000 total laser shots.

One experimental complication is the potential contamination of the images obtained in the two-color experiments by signal due to dissociation by the 225.65 nm probe radiation. Careful adjustment of the spatial overlap between the lasers, coupled with the high power of the photolysis pulse relative to the probe allowed images to be acquired with minimal probe contamination in most cases.

The time of flight (TOF) mass spectrum indicated signal corresponding to the following masses: N$^+$, NO$^+$, and NONO$^+$. The NO dimer signal was particularly strong when the lasers were probing the center of the molecular beam pulse. In order to avoid contamination of our images by signal originating from the dimer, we adjusted the nozzle timing such that only the low density, leading edge of the molecular beam was probed.

The wavelength calibration of our photolysis laser was checked by two photon dissociation of NO at the N($^2D_{5/2}$) $(2+1)$ REMPI resonance. The resulting mass 14 ion signal from both photolyzing NO and detecting the N($^2D_{5/2}$) photofragment with the same laser pulse allowed us to determine that the resonance was at 268.92 nm. According to the difference in term energies between the $^2S_{1/2}$ and the $^2D_{5/2}$ states as published by NIST,[33] the resonance should be at 269.0 nm. The observed 0.08 nm difference is consistent with the air to vacuum wavelength correction. All spectra are plotted against the two photon energy expressed in cm^{-1}, which incorporates the air to vacuum wavelength correction.

The NO$^+$ spectra in the region of the Rydberg states

$8d\pi^-(v=1)$, $6d\pi^-(v=1)/5s\sigma(v=3)$, and $5s\sigma(v=2)$ were obtained by monitoring the NO^+ signal using a photomultiplier tube (Hamamatsu 1P21) mounted near the phosphor screen while scanning the photolysis laser. Two photons of the photolysis laser were used to access the specific Rydberg state of NO, while a third photon ionized the molecule. The output of the photomultiplier tube was sent to a boxcar averager gated at the appropriate arrival time. The laser power was also measured with a photodiode and dye cell in order to normalize the NO^+ signal intensity for power fluctuations. Similarly, we also obtained a photofragment yield spectrum of NO in the $6d\pi^-(v=1)/5s\sigma(v=3)$ and $8d\pi^-(v=1)$ regions by monitoring the $O(^3P_2)$ signal while scanning the photolysis laser. In the $6d\pi^-(v=1)/5s\sigma(v=3)$ region, we undertook further diagnostics by scanning the photolysis laser for both linear and elliptical polarizations in order to better understand the observed spectral lines. We switched between elliptical and linear polarizations by using the combination of a rotatable double Fresnel rhomb and a right angled prism. For each transition observed in the $6d\pi^-(v=1)/5s\sigma(v=3)$ spectrum, a ratio of the linear versus elliptical polarization was obtained by integrating the overall signal for both cases and normalizing for the appropriate photolysis laser power.

The branching ratios for the fine structure states of $O(^3P_J)$ and $N(^2D_J)$ were measured by scanning the probe laser over the several resonances. Fluctuations in the laser energy were monitored and used to normalize the spectra after taking into account the power dependencies determined in separate experiments.

III. CALCULATIONS

This section outlines the method we used to calculate the angular distributions produced by photodissociation following two-photon excitation to NO Rydberg levels. We begin by providing a method for one-photon excitation of Hund's case (a) states, extend this to two-photon excitation of Hund's case (a) states, and then modify the result for two-photon excitation of Hund's case (b) states.

When predissociation from an excited state is slow on the time scale of rotation, one can expect that excitation to the state will exhibit resolved rotational structure. We first consider predissociation following one-photon excitation to a particular level via a selected rotational branch. The axial recoil approximation is assumed; that is, even though the predissociation may take a longer time scale than rotation, we assume that the energy released when the molecule eventually predissociates is sufficiently large that the products recoil nearly instantaneously with respect to rotation. For a diatomic molecule, this means that they recoil along the bond direction. We further assume that the angular distribution is unaffected by the competition between ionization and dissociation of the Rydberg level; that is, we assume either that the dissociation rate is much faster than the ionization rate at the laser intensities employed, or that ionization does not differentially affect the m_J distribution created by absorption to the Rydberg level.

The probability amplitude, A, for excitation in Hund's case (a) from level Ω'', J'', M'' to level Ω', J', M' is given by matrix elements that can be found in several references.[19,34] For excitation by linear polarization, there is no change in the projection of the rotational angular momentum onto the axis of linear polarization, which we will take to be the Z axis; that is $M'=M''$, and for simplicity we will denote either by M. Thus, $A(\Omega'',J'',\Omega',J',M)$ gives the probability amplitude for excitation of a rotational state J' making a projection M onto Z. For Hund's case (a), the projection of J' onto the molecular axis, z, is $\pm\Omega'$.

The remaining problem is to determine the distribution of angles θ between Z and z that is consistent with these two projections, because it is this distribution that, in the axial recoil limit, provides the distribution of product angles. The rotation matrix $d^{J'}_{M,\Omega'}(\theta)$ is normally described as the probability amplitude that if J' makes a projection of M onto an axis Z, it will make a projection Ω' onto an axis rotated from Z by an angle θ.[35] However, another way to view the rotation matrix is that it provides the probability amplitude for the distribution of angles θ consistent with having J' projections of M onto Z and Ω' onto z. Thus, the angular distribution for the products would then be given by

$$I(\theta)=\sum_M |A(\Omega'',J'',\Omega',J',M)d^{J'}_{M,\Omega'}(\theta)|^2. \quad (1)$$

A minor change in Eq. (1) should be made to account for the fact that the projection of J' onto z may be either $+\Omega'$ or $-\Omega'$. By the normal convention, the positive linear combination of these two projections is associated with the level of positive parity, while the negative combination is associated with negative parity. Thus, the angular distribution should properly be written as

$$I(\theta)=\sum_M |A(\Omega'',J'',\Omega',J',M)d^{J'}_{M,\pm\Omega'}(\theta)|^2, \quad (2)$$

where

$$d^{J'}_{M,\pm\Omega'}(\theta)\equiv\frac{d^{J'}_{M,\Omega'}(\theta)\pm d^{J'}_{M,-\Omega'}(\theta)}{\sqrt{2}}. \quad (3)$$

The extension of this formula to two-photon excitation of Hund's case (a) molecules is straightforward. Let the unprimed quantum numbers Ω, J, M be associated with the virtual intermediate state(s) through which the two-photon process occurs. Then the angular distribution of the photofragments is given by

$$I(\theta)=\sum_M \left|\sum_{\Omega,J}\frac{1}{(E(\Omega,J)-h\nu)}A(\Omega'',J'',\Omega,J,M)\right.$$
$$\left.\times A(\Omega,J,\Omega',J',M)d^{J'}_{M,\pm\Omega'}(\theta)\right|^2, \quad (4)$$

where the sum within the absolute value is over all possible intermediate electronic states and rotational levels.

We now modify Eq. (2) for Hund's case (b). In this coupling scheme, the electron spin, S, is uncoupled from the internuclear axis, while the total angular momentum for the final state, J', is given by the vector sum of S with N'. The projection of N' onto z is $\pm\Lambda'$. The probability amplitude for the two-photon transition depends on a sum over energy denominators and matrix elements for various intermediate states. For the case of a transition from a $^2\Pi$ (case a) through a $^2\Lambda$ (case b) intermediate to a $^2\Lambda$ (case b) final state, the two-photon probability amplitudes are given in Eqs. (2) and (3) of Ref. 18. In addition to the quantum numbers for the initial, intermediate, and final states, the transition amplitudes depend on ϵ'', the lambda doublet level of the initial state ($\epsilon''=1/-1$ for e/f levels), and η', which is equal to $+1$ for the $^2\Lambda^+$ component and -1 for the $^2\Lambda^-$ component. In analogy to the notation of Ref. 18, we denote the two-photon transition amplitudes, summed over energy denominators and intermediate states but prior to summing over M, as $D^{(2)}_{\Lambda',\eta'\leftarrow\Lambda'',\epsilon''}(J',N',J'',N'',M)$.

The complication of Hund's case (b) coupling is that the relationship between the z internuclear direction and the Z polarization direction is less straightforward. The vector J' still makes a projection of M onto Z, but now we need to calculate its projection onto z. However, J' is the vector sum of N' and S. N' makes a projection of $\pm\Lambda'$ onto z, whereas S makes a projection of $M_S=\pm\frac{1}{2}$. Consequently, J' must make a projection of $\pm\Lambda'\pm\frac{1}{2}$ onto z. The probability amplitude for having a particular value of this projection is simply the Clebsch–Gordon coefficient (N',Λ',S,M_S,J',M). The angular distribution of photoproducts for two-photon excitation to a case (b) state is thus

$$I(\theta)=\sum_M \left| D^{(2)}_{\Lambda',\eta'\leftarrow\Lambda'',\epsilon''}(J',N',J'',N'',M) \times\sum_{M_S}\left\{\begin{array}{c}(N',\Lambda',S,M_S,J',M)d^{J'}_{M,\Lambda'}(\theta)\\ \pm(N',-\Lambda',S,M_S,J',M)d^{J'}_{M,-\Lambda'}(\theta)\end{array}\right\}\right|^2, \tag{5}$$

where the + sign is for positive parity levels and the − sign for negative ones. We note in passing that the selection rules of Eq. (2) of Ref. 18 should be included in $D^{(2)}$ if the intermediate state is $^2\Sigma$.

IV. RESULTS

Our experimental efforts have concentrated on the O($^3P_2$) fragments formed in the photodissociation of different NO Rydberg states. We have investigated three different photolysis wavelength regions corresponding to the excitation of the $8d\pi^-(v=1)$, $6d\pi^-(v=1)/5s\sigma(v=3)$, and $5s\sigma(v=2)$ NO Rydberg states.

We first looked at the NO$^+$ spectra generated by scanning the photolysis wavelength in the regions indicated. These are shown in Fig. 1 along with the corresponding assignments. The spectra were obtained by using the photolysis laser as both an excitation and ionization source for the NO signal. Our results indicate that the NO$^+$ signal has a power dependence of 2.63 ± 0.07, typical of a $(2+1)$ REMPI process with a partially saturated ionization step. The $8d\pi^-(v=1)$ spectrum was taken with both 100% NO and 10% NO/He in order to vary the expansion conditions. The spectrum was assigned by assuming that the $8d\pi^-$ Rydberg state belongs to Hund's case (b), that the intermediate state is a $^2\Pi(b)$ state, and that the ground state of NO is purely Hund's case (a). The rotational constant for ground state was fixed at 1.696 cm^{-1},[36] and our calculated rotational constant for the upper state is 2.20 cm^{-1}. The spectrum was fitted using a spin splitting constant of zero. All of the spectral constants were obtained by adjusting the upper state values until a good fit was produced. Similarly, the $5s\sigma(v=2)$ spectrum has a straightforward assignment with a calculated upper state rotational constant of 1.93 cm^{-1}. The NO Rydberg state is a $^2\Sigma^+$ Hund's case (b), while the intermediate state is again a $^2\Pi(b)$ state, and the ground state is $^2\Pi(a)$. Table I shows our constants for all the different Rydberg states along with previously measured values.

As demonstrated in the past,[9,10] the NO spectral lines in the 269 nm region have been difficult to assign due to mixing of both the $5s\sigma(v=3)$ and the $6d\pi^-(v=1)$ Rydberg states of NO. In order to better understand this region, the NO spectrum was also taken with 100% NO so as to use different expansion conditions with increased rotational temperature. This spectrum is also shown in Fig. 1. The spectrum could not be attributed to either the $5s\sigma$ or the $6d\pi^-$ transition alone, but was a blend of transitions to both Rydberg levels, as well as an extra, unassigned line marked by an asterisk in Figs. 1(a) and 1(b). Our assignments were determined by employing the ion imaging technique as described later. We also made use of the results of the ratio between elliptical and linear polarizations to determine which lines have Q branch character. Integrated intensities of features scanned with linear and elliptical polarizations yielded ratios (linear/elliptical) of ~2/3 for all non-Q branch peaks in Fig. 1(a), ~1.5 for the dominant $6d\pi^-$ Q_{21} peak, and ~1 at the positions of the other Q_{21} lines and at the $6d\pi^-$ Q_{11} bandhead. We also observed NO$^+$ signal that was not dependent on the excitation laser wavelength and therefore not dependent on the rotational level and rotational branch accessed. This signal formed an underlying broad baseline in the spectra, and it was especially strong in the $6d\pi^-(v=1)/5s\sigma(v=3)$ region.

Further information can be extracted from the spectra, yielding the rotational temperature of our expansion. The temperature is calculated using the intensities of the peaks present in the spectra along with the line strengths for each of the transitions. The intensities are obtained by fitting Gaussians to the peaks of interest. In the case of blended lines, a deconvolution is performed using a sum of Gaussians. The line strengths used correspond to the transitions which involve a Π intermediate state. The slope of the Boltzmann plot, an example of which is shown in Fig. 2 gives the desired rotational temperature. For the 10% NO expansion we measured a rotational temperature of 9 ± 1 K from the $5s\sigma(v=2)$ spectrum and 11 ± 5 K from the $6d\pi^-(v=1)/5s\sigma(v=3)$ spectrum. For the 100% NO expansion the $8d\pi^-(v=1)$ spectrum gives a rotational temperature of 35 ± 4 K, while the $6d\pi^-(v=1)/5s\sigma(v=3)$ spectrum yields a value of 36 ± 12 K.

Figure 3 shows the yield spectrum for the $6d\pi^-(v=1)/5s\sigma(v=3)$ region measured by monitoring the O atom fragment through the $(3p\ ^3P_{2,1,0}\leftarrow\leftarrow 2p\ ^3P_2)$ transition. The predissociation signal is a result of two-photon excitation of

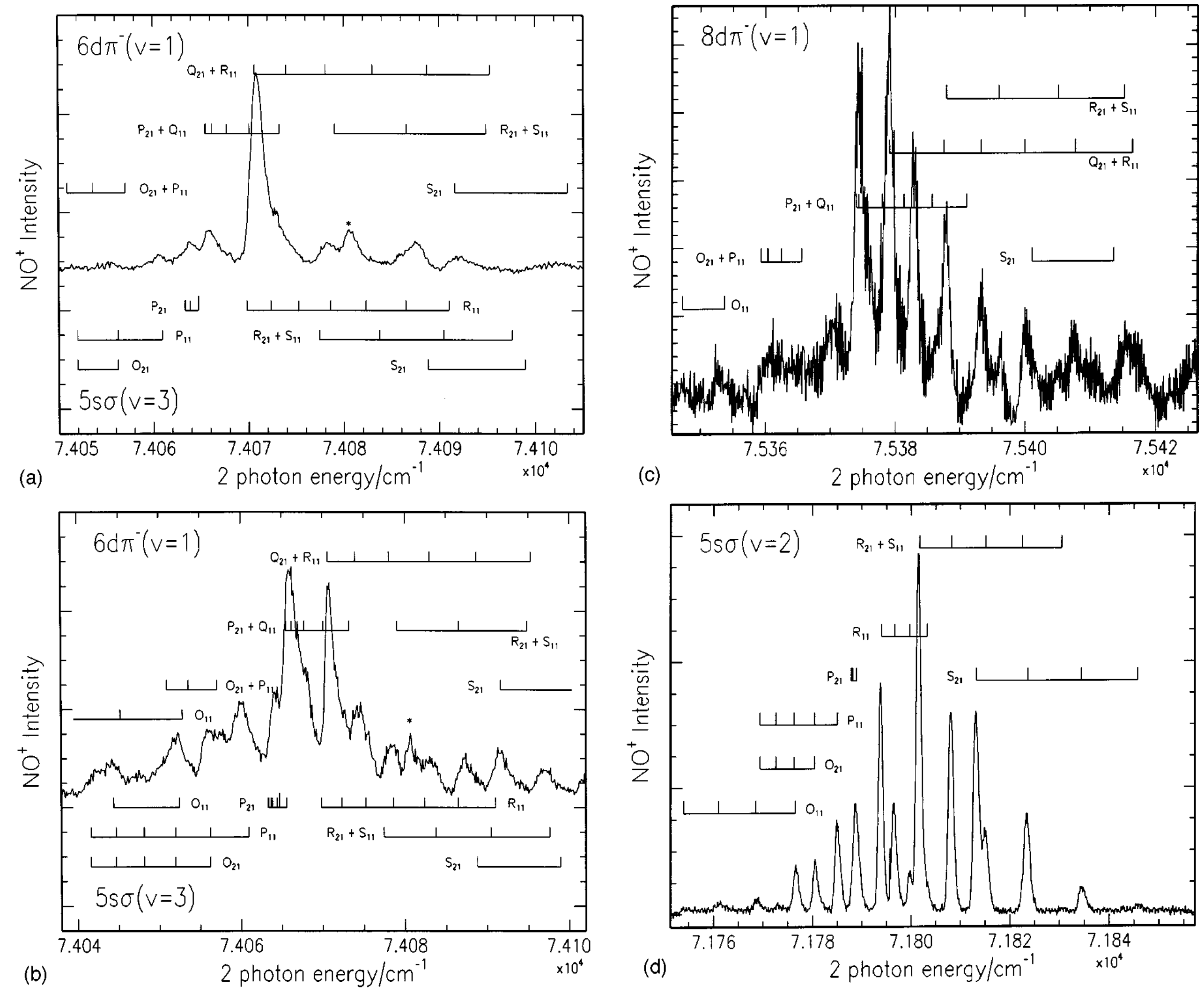

FIG. 1. Two-photon ionization spectra of NO as a function of the two-photon energy. (a) Ionization of the $6d\pi^-(v=1)/5s\sigma(v=3)$ bands using 10% NO in He. Top assignments correspond to $6d\pi^-(v=1)$, while bottom assignments belong to $5s\sigma(v=3)$. (b) Ionization of the $6d\pi^-(v=1)/5s\sigma(v=3)$ bands using 100% NO. (c) Ionization of the $8d\pi^-(v=1)$ band using 100% NO. (d) Ionization of the $5s\sigma(v=2)$ band using 10% NO in He. The assignments were made using the spectroscopic constants present in Table I.

the Rydberg state followed by a (2+1) probe step of the atomic oxygen fragment. It is noted by comparison of the O^+ action spectrum to the NO^+ spectrum that some of the transitions in the NO^+ spectrum do not have matching intensities in the action spectrum. This observation indicates that the spectra are the result of competition between ionization and dissociation of the Rydberg accessed by two-photon absorption. Because there is rotational structure, the dissocia-

TABLE I. Spectroscopic constants used in assigning the $8d\pi^-(v=1)$, $6d\pi^-(v=1)/5s\sigma(v=3)$, and the $5s\sigma(v=2)$ NO Rydberg bands. Also included are constants from previous work.

	This work			Previously measured		
State	B' (cm^{-1})	Gamma	T_v (cm^{-1})	B' (cm^{-1})	Gamma	T_v (cm^{-1})
$8d\pi^-(v=1)$	2.20	0.07	75 376.0	2.20[a]	0.0[a]	75 382.0[a]
$6d\pi^-(v=1)$	2.10	0.0	74 067.7	2.10[b]	0.0[b]	74 048.0[b]
				2.10[c]	0.0[c]	74 069.7[c]
$5s\sigma^-(v=3)$	1.90	0.0	74 067.3	1.90[d]	0.0[d]	74 077.0[d]
				1.90[c]	0.0[c]	74 073.3[c]
$5s\sigma^-(v=2)$	1.93	0.0	71 791.4	1.93[e]	0.0[e]	71 792.0[e]

[a] Obtained from Pratt *et al.* (Ref. 18).

[b] Calculated by interpolation based on values given by Pratt *et al.* (Ref. 18).

[c] Obtained from Umemoto *et al.* (Ref. 23).

[d] Calculated by extrapolation based on the values given by Miescher *et al.* (Ref. 1).

[e] Obtained from Miescher *et al.* (Ref. 1).

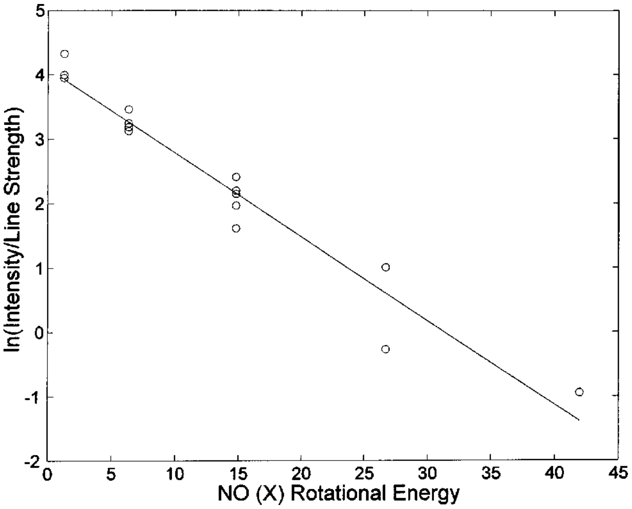

FIG. 2. Boltzmann plot for the $5s\sigma(v=2)$ region.

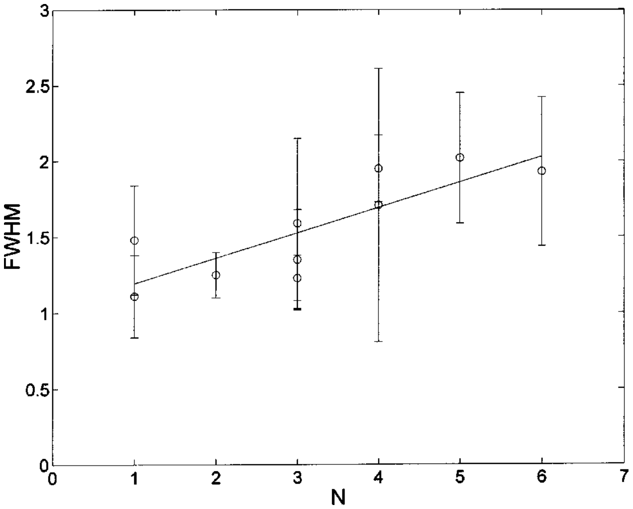

FIG. 4. Full width at half maximum (cm^{-1}) as a function of the N' rotational quantum number obtained from the $8d\pi^-(v=1)$ band region.

tion lifetime is longer than a rotational period, about 10^{-12} s. To compete with ionization, which happens in less than the laser pulse width, the dissociation must occur in less than about 10^{-8} s. The line strengths corresponding to transitions through a Π intermediate state along with the peak intensities in the action spectrum reveal that the $5s\sigma(v=3)$ Rydberg state is more strongly predissociative than the $6d\pi^-(v=1)$ Rydberg state. The O^+ action spectrum also provides a measurement of the rotational temperature, which we find to be 15 ± 3 K, in good agreement with the NO^+ spectrum.

In the $8d\pi^-(v=1)$ NO Rydberg state region, there were no apparent differences in the intensities of features in the O photofragment yield spectrum compared to those in the NO REMPI spectrum. However, we observed an increase of the full width half maximum (FWHM) of the transitions with an increase of the upper state N' quantum number, as shown in Fig. 4. A model calculation, which fit the data, showed that the broadening was due to a small but non-zero spin splitting constant. In the $5s\sigma(v=2)$ region, this broadening trend is negligible, so that we assumed a spin splitting constant of zero. The γ values for the different Rydberg state regions are included in Table I.

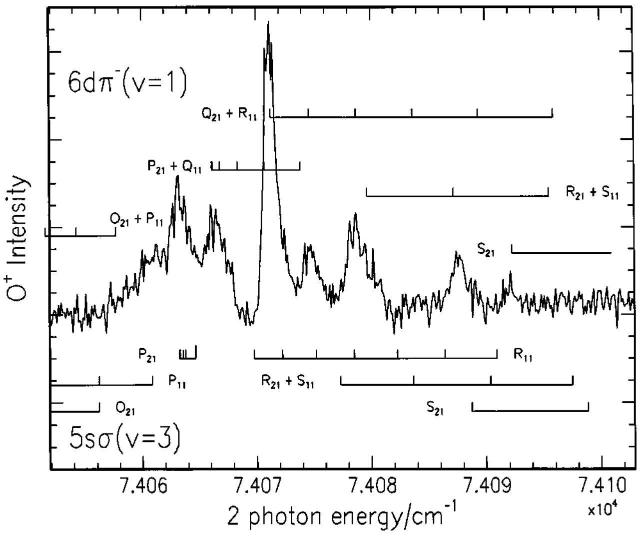

FIG. 3. Photofragment yield spectrum of NO $6d\pi^-(v=1)/5s\sigma(v=3)$ bands. Top assignments correspond to $6d\pi^-(v=1)$ and the bottom ones to $5s\sigma(v=3)$.

To better understand the dynamics of these NO Rydberg states, images of the velocity distributions of the $O(^3P_2)$ fragments were taken at wavelengths corresponding to many of the rotational levels and rotational branches observed for the three different Rydberg regions. As noted before, some of the NO transitions had weaker intensities in the action spectrum, which reduced the photodissociation product yield and inhibited our ability to take images on some of the transitions. Figure 5 shows representative raw images taken on the $Q_{21}+R_{11}$ $(J=0.5)$ progression in the $8d\pi^-(v=1)$, $6d\pi^-(v=1)/5s\sigma(v=3)$, and $5s\sigma(v=2)$ regions. In these images the electric vectors of the dissociation and ionization lasers are pointing in the same direction, parallel to the face of the microchannel plate detector and in the vertical direction of Fig. 5.

The product imaging technique makes use of an inverse Abel transform to reconstruct the three-dimensional velocity distribution from its two-dimensional projection.[27,28] The $O(^3P_2)$ velocity distributions recovered from the inverse Abel transform can be separated into angular and speed components. Angular distributions are determined by integrating over the desired speed for each angle, while the speed distribution is achieved in a similar manner by integrating over all angles for each speed. The speed distributions can be further transformed, using the law of conservation of linear momentum, into total translational energy distributions for $NO \rightarrow N(^2D_{5/2})+O(^3P_2)$ dissociation. The kinetic energy distributions together with a comb indicating the energy of the possible N atomic states formed in conjunction with $O(^3P_2)$ are also shown in Fig. 5. Examination of the energy distributions corresponding to the images taken in the three NO Rydberg regions shows that the main predissociation channel yields $N(^2D_{5/2})$ and $O(^3P_2)$ fragments. Some of the images revealed that some $O(^3P_2)$ fragments possess a broad, weak distribution of higher translational energy. This signal is

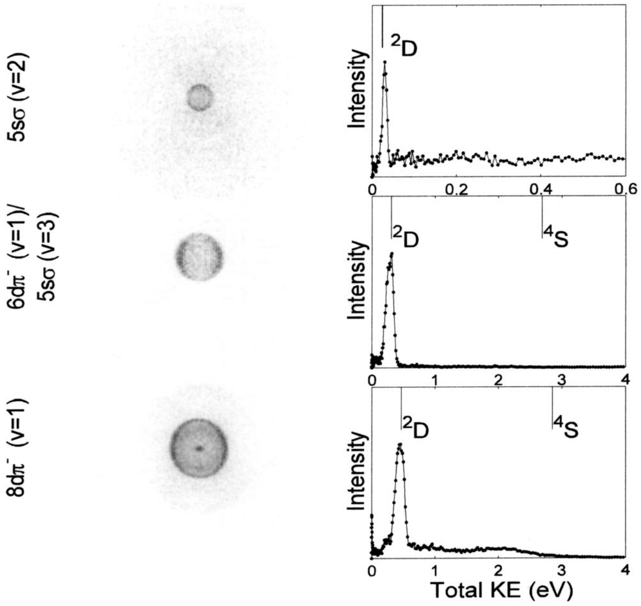

FIG. 5. Representative raw images obtained in the three different NO Rydberg regions along with the corresponding energy distributions. The $5s\sigma(v=2)$ image is taken on the $Q_{21}+R_{11}$ $(J=0.5)$ rotational line; the $6d\pi^-(v=1)/5s\sigma(v=3)$ image is taken on the $Q_{21}+R_{11}$ $(J=0.5)$ $6d\pi^-/Q_{21}+R_{11}$ $(J=1.5)$ $5s\sigma$ blended line, and the $8d\pi^-(v=1)$ image belongs to the $Q_{21}+R_{11}$ $(J=0.5)$ rotational transition. The combs in the energy distributions represent the energetics corresponding to the formation of N(^2D) and N(^4S) counterfragments.

mainly due to one color photodissociation of NO by the probe laser at 225.65 nm, but also due to the two-photon photodissociation of the NO dimer, which contributes to the broadening of the peak, as discussed below.

The more interesting features observed in the images are the angular distributions. Because the distribution is produced by a two-photon absorption process, we fit the angular distributions to both an anisotropy parameter, β, and higher order term, γ: $I(\theta)\propto 1+\beta P_2(\cos\theta)+\gamma P_4(\cos\theta)$. The β and γ values for every wavelength imaged are given in Table II along with error ranges assigned by the following procedure. At each wavelength multiple images were taken. Each image was then analyzed independently to obtain separate values for β and γ, and the spread was used as an error range for that particular dissociation wavelength. The angular distributions were finally obtained from the sum of the images at each wavelength. It can be observed that the angular distributions are very dependent on the particular transition probed in the NO Rydberg spectra. This observation led us to further investigate how photofragment angular distributions from one-photon and two-photon transitions depend on the rotational level and the rotational branch excited, as described in the calculation section above. The results of these calculations are also included in Table II. We were also able to image the products originating from the NO signal that was independent of the photolysis wavelength. As discussed above, this contributed to an overall NO baseline in the Rydberg spectra. Although the product yield was very small, we increased the overall detection efficiency by using a

TABLE II. β and γ parameters obtained by fitting $I(\theta)\propto 1+\beta P_2(\cos\theta)+\gamma P_4(\cos\theta)$ to both the experimental and theoretical angular distributions for each rotational transition imaged in the three different NO Rydberg regions.

			Experiment		Theory	
State	λ_{air} (nm)	Assignment	Beta	Gamma	Beta	Gamma
$8d\pi^-(v=1)$	265.22	$Q_{21}+R_{11}(J=2.5)$ $S_{11}+R_{21}(J=0.5)$	0.47 ± 0.01	-0.16 ± 0.08	0.53	-0.16
	265.24	$Q_{21}+R_{11}(J=1.5)$	0.30 ± 0.10	-0.10 ± 0.01	0.34	0.017
	265.25	$Q_{21}+R_{11}(J=0.5)$	-0.43 ± 0.07	-0.21 ± 0.10	-0.04	0
	265.27	$Q_{11}+P_{21}(J=1.5,2.5,3.5)$	-0.09 ± 0.06	-0.13 ± 0.11	-0.13	-0.008
$6d\pi^-(v=1)/$ $5s\sigma(v=3)$	269.85	$S_{21}(J=0.5)$ $6d\pi^-$	0.85 ± 0.30	0.01 ± 0.15	0.86	0.14
	269.87	$S_{11}+R_{21}(J=1.5)$ $6d\pi^-$ $S_{21}(J=0.5)$ $5s\sigma$	0.54 ± 0.20	-0.16 ± 0.11	0.69	0.08
	269.90	$Q_{21}+R_{11}(J=2.5)$ $6d\pi^-$ $Q_{21}+R_{11}(J=3.5)$ $5s\sigma$	0.64 ± 0.06	-0.04 ± 0.04	0.52	-0.002
	269.92	$Q_{21}+R_{11}(J=1.5)$ $6d\pi^-$ $Q_{21}+R_{11}(J=2.5)$ $5s\sigma$	0.44 ± 0.09	-0.14 ± 0.05	0.34	-0.007
	269.93	$Q_{21}+R_{11}(J=0.5)$ 30% $6d\pi^-$ $Q_{21}+R_{11}(J=1.5)$ 70% $5s\sigma$	-0.13 ± 0.11	-0.36 ± 0.06	0.09	-0.28
	269.95	$Q_{11}+P_{21}(J=3.5)$ $6d\pi^-$	0.80 ± 0.19	-0.19 ± 0.18	0.5	0.02
	269.96	$Q_{11}+P_{21}(J=1.5)$ $5s\sigma$	1.37 ± 0.19	0.20 ± 0.20	0	0
	269.97	$P_{11}(J=1.5)$ $5s\sigma$	1.42 ± 0.20	0.09 ± 0.14	0	0
$5s\sigma(v=2)$	278.42	$S_{21}(J=0.5)$	0.41	0.20	0.86	0.14
	278.44	$S_{11}+R_{21}(J=1.5)$	0.46	0.03	0.71	-0.23
	278.46	$S_{11}+R_{21}(J=0.5)$	0.83 ± 0.13	0.27 ± 0.01	1.06	0.34
	278.49	$Q_{21}+R_{11}(J=0.5)$	0.66 ± 0.05	-0.03 ± 0.01	1.00	0
	278.51	$Q_{11}+P_{21}(J=0.5,1.5,2.5)$	-0.035	-0.08	-0.096	0
	278.53	$P_{11}(J=1.5)$	1.07 ± 0.02	0.11 ± 0.07	0	0
	278.56	$O_{11}(J=2.5)$, $O_{21}(3.5)$ $P_{11}(J=3.5)$	0.02 ± 0.05	-0.01 ± 0.02	-0.02	-0.008

single wavelength on the N($^2D_{5/2}$) resonance to act as both photolysis and probe. In the N($^2D_{5/2}$) resonance region the NO signal observed was independent of the photolysis wavelength. For this particular region, based on the angular distribution of the N($^2D_{5/2}$) fragment, we measured an anisotropy parameter $\beta = 0.53$.

Finally, we measured the ratio of O(^3P_J) spin–orbit populations at 270.01 nm, which corresponds to the $Q_{21} + P_{11}$ ($J = 1/2$) transition in the $6d\pi^-(v=1)$ region. At this wavelength we found that $(^3P_2):(^3P_1):(^3P_0) = (0.75 \pm 0.13):(0.22 \pm 0.06):(0.03 \pm 0.01)$. The branching ratio of the two spin–orbit states of the N(^2D) was also measured to be N($^2D_{5/2}$):N($^2D_{3/2}$)$= 1.8 \pm 0.3$.

V. DISCUSSION

A. Energy distributions

Two-photon excitation from the *d*-like highest occupied molecular orbital of the NO ground state is enhanced to the atomiclike Rydberg states with *s* or *d* character. We have excited Rydberg states of NO in the energy region below the ionization potential but above the limits to the following dissociation channels:

$$\mathrm{NO} \rightarrow \mathrm{N}(^2D) + \mathrm{O}(^3P) \quad E_{\mathrm{threshold}} = 8.876 \ \mathrm{eV}, \tag{6}$$

$$\mathrm{NO} \rightarrow \mathrm{N}(^4S) + \mathrm{O}(^1D) \quad E_{\mathrm{threshold}} = 8.463 \ \mathrm{eV}, \tag{7}$$

$$\mathrm{NO} \rightarrow \mathrm{N}(^4S) + \mathrm{O}(^3P) \quad E_{\mathrm{threshold}} = 6.496 \ \mathrm{eV}. \tag{8}$$

Detection of O(^3P) allows us to monitor both channels (6) and (8), whereas detection of N(^2D) provides information only about channel (6). The lowest excitation energy used in this study, 8.92 eV, which corresponds to the $5s\sigma(v=2) \leftarrow X$ transition, is only 0.04 eV above the threshold for channel (6), whereas, the shortest wavelength excitation, the $8d\pi^-(v=1) \leftarrow X$ transition, is 0.48 eV above the threshold. In Fig. 5, it is evident that the production of N(^2D) is the dominant channel in the three spectral regions investigated. In each image there is only one main ring corresponding to the kinetic energy of N(^2D)+O(^3P) fragments. The relatively flat, but nonzero, background at the higher kinetic energy comb position corresponding to channel (8) indicates that there may be, at best, only a very minor contribution from the N(^4S)+O(^3P) products.

Bakker *et al.* observed both channels (6) and (8) in the wavelength region near 275 nm.[26] They concluded that the N(^2D) channel dominated when the $4d\pi^-(v=2)$ and the $5d\pi^-(v=1)$ Rydberg levels were excited and that the N(^4S) channel dominated when Rydberg levels lying some 20–30 cm^{-1} lower in energy than these $nd\pi^-$ bands were excited. They speculated that these redshifted features might be the $nd\pi^+$ levels which are expected to shift by interaction with $nd\sigma$ levels by the same amount. Previous studies, which only detected N(^2D), had failed to observe these levels, and it was assumed that they were strongly predissociated in channel (8). In the vicinity of the $6d\pi^-(v=1)$ transition, we do not see other bands nor a similarly strong contribution from the N(^4S) product channel despite scanning ~40 cm^{-1} to the red of the band origin. The absence of bands in this region may be due to our limitation of the photolysis laser energy to less than 1 mJ/pulse. Bakker *et al.* reported using photolysis laser energies between 2–8 mJ/pulse.[26] The appearance of their spectra shows substantial power broadening and loss of rotational resolution compared to previous work, which they attributed to having to use high laser energies to produce fragments efficiently. We did observe, however, a weak band to the red of and partially overlapped with the $8d\pi^-(v=1)$ *O* and *P* branches. The appearance of the spectrum was different from the $nd\pi^-$ spectra but very similar to that of the $5s\sigma$ spectrum. Analysis yielded an anomalously large rotational constant of 2.50 cm^{-1} and a band origin of 75 318.5 cm^{-1}. We tentatively assign this region as the $8d\sigma$ band.

In the $8d\pi^-(v=1)$ images, additional rings appear which are due to dissociation of NO or NO dimer at the two-photon energy of the probe laser at 225.65 nm. These faint rings appear in the probe-alone signal and are also present for excitation of the other Rydberg levels excited by the pump laser, but due to the stronger dissociation signal from the photolysis laser at these wavelengths, the probe laser contribution was made to be negligible by reducing the probe laser pulse energy. The additional rings agree well with the energetics of dissociation at two photons of 225.65 nm to yield products from channel (6) above and from an additional channel,

$$\mathrm{NO} \rightarrow \mathrm{N}(^2P) + \mathrm{O}(^3P) \quad E_{\mathrm{threshold}} = 10.072 \ \mathrm{eV} \tag{9}$$

and correspond to features in the energy distributions at 2.11 and 0.92 eV, respectively. The measured power dependence of the probe laser generated signal yielded a slope of 4.4 $\pm$ 0.4 for the plot of ln (signal intensity) versus ln (laser energy), which is consistent with a two-photon excitation of NO followed by a second two-photon absorption by the atomic oxygen fragment and a partially saturated ionization step in the (2+1) REMPI detection scheme. The peak corresponding to 2.11 eV in the energy distributions is especially broad, and even though the energetics agree well with the formation of O($^3P_2$) and N(^2D) from the one color two-photon dissociation of NO at 225.65 nm, the increase in the width of the peak indicates that the process is not the simple dissociation of a diatomic precursor from a single energy level. The broad distributions reveal that the counterfragment of the O(^3P) atomic fragment has some wider distribution of internal energy.

Our TOF spectra indicate the presence of NONO$^+$, from which we conclude that the NO dimer formation occurs. The dissociation energy of the dimer is very small in comparison to the dissociation energy of the NO molecule. In the gas phase dimer the NO ground-state monomers are bound by 710 $\pm$ 40 cm^{-1}.[37] Several causes for the broadening of the O(^3P) peak at 2.11 eV in the energy distributions are plausible. According to East *et al.*,[37] there are no dimer states that can be accessed above 0.86 eV, and therefore the possibility of the dimer dissociating at 225.65 nm (5.5 eV) to produce two NO molecules is ruled out. Furthermore, at 225.65 nm we are above the ionization potential of the NO dimer, as shown by Urban *et al.*,[38] but calculations done by East *et al.*[37] indicate that all the asymptotes are ionic. This implies that the $NONO^+$ dimer cation cannot play a role in the formation of NO molecules that retain internal energy and cause a broadening of our peak.

The more likely cause of the broadening could involve two-photon absorption of the dimer to produce an electronic state in which one of the monomers is excited to a Rydberg state. This dimer state might then dissociate directly to produce $O(^3P)$ and $N(^2D)$ fragments along with a NO molecule. Since the dissociation energy would be dominated by the NO molecule dissociation and not by the much weaker dimer dissociation, the feature at 2.11 eV would be expected to agree well with the NO photolysis process, as observed, but it would be broadened because of the partitioning of energy between the two NO monomers as the dimer dissociated.

B. Rydberg state spectral assignments

Jet-cooled NO was excited from the lower spin component of the ground state ($X\,^2\Pi_{1/2}$) to four different Rydberg states just below the ionization limit using a two-photon excitation scheme with wavelengths in the 265–278 nm region. Absorption of a third photon within the same excitation laser pulse ionized the NO Rydberg levels and allowed detection of the resulting NO^+ by TOF MS. In the spectral region corresponding to two-photon energies near 74 070 cm^{-1}, previous studies have indicated that there are overlapping transitions to the $5s\sigma(v'=3)$ and $6d\pi^-(v'=1)$ Rydberg states.[18,22,23,31] In an effort to sort out this overlapped region, several strategies have been employed. Clean spectra of the type "$s\sigma$" and "$d\pi^-$" were obtained for comparison purposes with the features of the blended region. The rotational constants and the vibronic term energies obtained from our analysis of these clean spectra agreed well with the literature values. Comparison of the blended region with the clean spectra became useful at warmer expansion temperatures where it was apparent that the lower frequency side of the $5s\sigma(v'=3)/6d\pi^-(v'=1)$ spectrum displayed the "$s\sigma$" pattern while the "$d\pi^-$" pattern dominated at the higher frequencies.

A second strategy to assign the overlapped spectra of the $5s\sigma(v'=3)$ and $6d\pi^-(v'=1)$ region involved switching the polarization of the laser used to excite and ionize the NO Rydberg levels from linear to elliptical. Subsequent scans over the features of the spectra with the two polarizations show intensity differences analogous to those predicted by Bray and Hochstrasser for circular and linear polarization.[19] Only for Q-branch transitions with $\Delta\Omega=0$ will the ratio of intensities with linear to circular polarization depart from a value of 2/3. The condition that $\Delta\Omega=0$ is satisfied since the jet-cooling of the NO populates only the $\Omega=1/2$ spin–orbit manifold in the ground state and the $5s\sigma$ (or $S\,^2\Sigma^+$) Rydberg state has $\Omega=1/2$ by definition. The $6d\pi^-$ Rydberg state has both $\Omega=1/2$ and 3/2 levels. We assume that elliptical polarization has similar qualitative effect to circular polarization. By this method, Q branch character or partial Q branch character due to overlapping non-Q branch lines was established for several features in the spectrum. However, overlap with non-Q branch lines will reduce the overall polarization intensity ratio. These Q-branch lines were assigned to the $6d\pi^-$ Rydberg level since the two-photon line strengths for the $5s\sigma$ Q branches were calculated to be zero at low J. Spectra taken with warmer expansion conditions clearly revealed the formation of a bandhead at the position of the lowest two-photon frequency of the indicated Q branch lines.

The third strategy employed to assign the blended $5s\sigma(v'=3)$ and $6d\pi^-(v'=1)$ spectral features again made use of comparison with information from the clean "$s\sigma$" and "$d\pi^-$" regions, namely, the angular distributions of the O atom predissociation product. Addition of a second laser used to detect atomic oxygen by REMPI, coupled with ion imaging of the product velocity distribution, yielded angular distributions which are highly dependent on both the rotational branch and quantum number of the excited Rydberg level, as well as the electronic symmetries involved in the transition. Although the intensity distribution in the action spectrum differed significantly from the NO^+ spectrum, there was a clear correspondence between the spectral features. In this way, the majority of the features in the blended region were assigned to be "$d\pi^-$"-like, since the angular distributions were very similar to those obtained from imaging the predissociation products after excitation to the $8d\pi^-$ Rydberg state. Only two features were sufficiently intense in the action spectrum to be cleanly assigned to be "$s\sigma$"-like.

Spectral assignments were then made quantitative by calculating the two-photon wave numbers corresponding to the difference in term energies calculated for a case (a) ground state and a case (b) final state. The upper state rotational constant, spin-splitting constant, and the electronic plus vibrational energy were varied, while keeping the ground state rotational constant fixed until a good fit of the assignments to the peak positions was obtained. The assignments were in agreement with the results of the polarization study which distinguished between Q- and non-Q-branch transitions. By changing the conditions of the expansion, "warmer" spectra could be obtained with additional features extending to higher rotational quantum numbers. The spectral constants were shown to be adequate to describe these additional spectra. In all cases γ, the spin-splitting constant for the upper state, was found to be negligible.

The two-photon energies in cm^{-1} were calculated from the laser wavelength after conversion from air to vacuum. The laser wavelength was shown to be accurate within 0.01 nm near 269 nm by calibration against the $N(^2D)(2+1)$ REMPI transition at 74 357.086 cm^{-1}. This is well within the laser manufacturer's specifications for accuracy within 0.05 nm at a laser fundamental of 580 nm. In terms of two-photon energies, the stated laser accuracy works out to ± 6 cm^{-1} at 74 000 cm^{-1}. The agreement of the electronic plus vibrational term energies obtained in this work with those from the literature is within 6 cm^{-1} in each case.

Both Umemoto and Matsumoto,[23] and Gadd *et al.*,[22] have published partial spectral assignments for the blended $5s\sigma(v'=3)$ and the $6d\pi^-(v'=1)$ region based on unpublished single VUV photon absorption work by Dressler and Miescher. In both cases the spectra were considerably hotter than in this work and therefore considerably congested.

Apart from observing several extra lines, Gadd assigned the region completely to the $5s\sigma(v=3)$ Rydberg transition. Due to the low resolution and high congestion in Gadd's spectrum, comparison with our spectra is not useful. In the higher resolution experiments of Umemoto and Matsumoto, in which the $N(^2D)$ predissociation product yield was monitored by REMPI as the excitation laser was scanned across the Rydberg absorption, the much greater detail revealed a prominent role for the $6d\pi^-$ transition. They assigned two main progressions to the $6d\pi^-$ Q_{11} and Q_{21} branches following Pratt's study of the $nd\pi^-$ spectra. Their assignment of $5s\sigma$ features, however, was based on unpublished line positions for the R_{11} and R_{21} branches, extrapolation of Q_{11} and P_{11} lines positions from lower vibrational bands, from which they then calculated the S_{21} branch line positions, and the Q_{11} bandhead position from single-photon work. Not surprisingly, the resulting $5s\sigma$ assignments did not match well with the spectrum. Consequently, the role of the $5s\sigma$ Rydberg state in the predissociation was not clearly defined, and several $5s\sigma$ lines were mistakenly assigned to the $6d\pi^-$ band. In the high resolution scan in their Fig. 3, for example, the lines assigned as $6d\pi^-$ Q_{11} (3/2, 5/2, and 7/2) are actually the $5s\sigma$ $R_{11}(J=1/2)$, the $6d\pi^-$ $Q_{21}(J=1/2)$, and the $5s\sigma$ $R_{11}(J=3/2)$ lines, respectively.

We reanalyzed the $N(^2D)$ yield spectra of Figs. 2 and 3 of Ref. 23. The energy comb spacings for the $5s\sigma$ R_{21} and the $6d\pi^-$ Q_{21} branches reveal that the same upper state rotational constants were used as in this work, 1.90 and 2.10 cm^{-1}, respectively. We find that both the $5s\sigma$ and the $6d\pi^-$ assignments, however, should be shifted to the red by approximately 10 and 4 cm^{-1}, respectively, based on the positions of the $5s\sigma$ Q_{11} and the $6d\pi^-$ Q_{21} branches. Similar shifts of 8.8 and 2.5 cm^{-1}, are predicted from a comparison of the electronic and vibrational term energies obtained here and from their assignments for the same $5s\sigma$ Q_{11} and the $6d\pi^-$ Q_{21} branches. At the very high resolution provided by the spectrum in their Fig. 3, we were not only able to assign the main features to both $6d\pi^-$ Q_{21} and the $5s\sigma$ R_{11} branches but also the small peaks to S_{11} and S_{21} transitions from both Rydberg levels.

Several differences are readily observed in the intensities of corresponding features in the NO^+ spectrum and the O photofragment yield spectrum for this region. The relative intensities of the $5s\sigma$ P_{21} and the $6d\pi^-$ Q_{11} branch heads [denoted as $5s\sigma$ $P_{11}(J=3/2,5/2)$ in Fig. 2 of Ref. 23], favor the $5s\sigma$ band in both the $N(^2D)$ yield spectrum and our $O(^3P)$ yield spectrum, whereas the trend is the opposite in the NO^+ spectra. This illustrates the differences in competition between predissociation and ionization for the two Rydberg levels clearly observed in both the spectra of Umemoto and Matsumoto and ours. Similar differences appear at other transitions as well and give rise to the scatter in the Boltzmann plots and the resulting high uncertainties in the rotational temperatures for the two expansions $(11\pm5;36\pm12\ \mathrm{K})$. By contrast, the corresponding uncertainties in the rotational temperature and the scatter in the Boltzmann plots from the $8d\pi^-$ $(35\pm4\ \mathrm{K})$ and the $5s\sigma(v=2)$ $(9\pm1\ \mathrm{K})$ data are much reduced. The relative efficiencies of the competing pathways also appear to be affected by the NO internal energy. The scatter of data in the Boltzmann plots resolves into two parallel, but separate lines corresponding to the $6d\pi^-$ and the $5s\sigma$ contributions at temperatures near 30 K, with the $5s\sigma$ component having the greater contribution to the NO^+ spectrum, whereas, at lower temperatures, the two Rydberg levels showed similar intensity distributions.

The competition between ionization and dissociation of NO Rydberg states can greatly influence the appearance of the excitation spectra. In the limit of direct dissociation or of predissociation that is much faster than the molecular rotational period, lifetime broadening of the energy levels causes all the rotational branches to be excited coherently. Consequently, rotational structure is washed out in the absorption spectrum. In circumstances when the timescale of predissociation approaches or is longer than that of the molecular rotation, then the spectrum will show rotational structure. In the case of NO Rydberg levels with low rotational quantum numbers $N'=0-5$ as in this work, the rotational period is on the order of 10–1 ps, respectively. Since we observe both dissociation products and molecular ions with well-defined rotational structure in the corresponding O action and NO^+ REMPI spectra, then broad limits can be set on the predissociation lifetime. The ionization process involves the absorption of a third photon following the two-photon excitation to the Rydberg level, a process which must occur within the 5–10 ns duration of the laser pulse. This provides an upper limit on the dissociation lifetime. The several picosecond rotational period provides the lower limit.

The widths of the spectral features in either the NO^+ or O action spectra contain several contributions besides the effect of lifetime broadening. The laser bandwidth contributes approximately 0.4 cm^{-1}. In a power dependence study of the $6d\pi^-(v=1)$ $Q_{21}(J=\frac{1}{2})$ transition, power broadening by the laser further increased the spectral width up to a factor of two at the maximum laser energy used. Doppler broadening of the NO absorption is small due to the cold temperature in the expansion, about 0.03 cm^{-1}, for the REMPI spectrum. For the O action spectrum, however, the Doppler component should be substantial since the width [0.77 cm^{-1} for the $6d\pi^-(v=1)$ $Q_{21}(J=\frac{1}{2})$] reflects the energy released in the dissociation process. Convolution of the laser bandwidth with the effects of power and Doppler broadening yields a FWHM of 0.8 (NO REMPI) and 1.1 cm^{-1} (O action). Peaks in the O action spectrum are generally wider than in the NO REMPI spectra, but the widths are not reliable due to problems in maintaining the laser overlap across the scan as well as the finite band width of the probe laser used to detect the O atoms.

Our spectra, especially in the $8d\pi^-(v=1)$ region, suggest an increase in the FWHM with an increase of the upper state N' quantum number. Figure 4 shows that the linewidths linearly increase by a factor of 2 in going from $N'=1$ to $N'=6$. The minimum width at $N'=1$ of 1.1 cm^{-1} reflects the contributions mentioned above as well as any spin–splitting or lifetime broadening effects. Our Gaussian model of spin splitting dependence on N' predicts a spin–splitting constant of 0.07 cm^{-1} when fitted to the data of Fig. 4, which would broaden $N'=1$ levels by 0.1 cm^{-1}. This small amount can be neglected leaving the difference between the observed

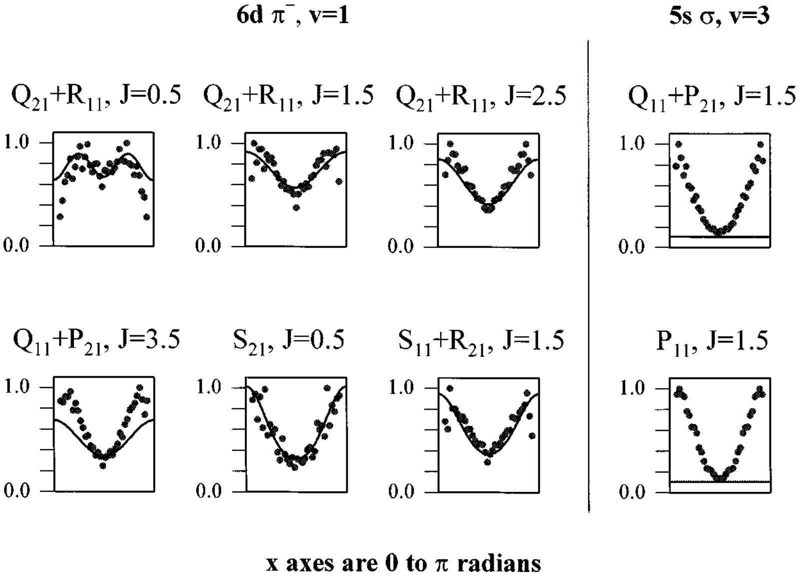

FIG. 6. Graphical representation of the theoretical angular distribution (solid line) in comparison to the experimental angular distributions (data points) for the $6d\pi^-(v=1)/5s\sigma(v=3)$ region.

minimum width and that estimated above from laser and Doppler broadening to arise from lifetime broadening. A crude deconvolution would result in a lifetime broadening contribution of 0.75 cm^{-1}. This would correspond to a dissociation lifetime of 7 ps. The semiclassical rotational period for $N'=1$, given a rotational constant of 2.2 cm^{-1} is about 5 ps. These values are in agreement with the scenario suggested above in which the predissociation process is slightly slower than the rotational period, thus allowing rotational structure to be observed.

C. Dissociation product angular distributions

The rotational resolution in the Rydberg excitation spectra allows an investigation of how the NO Rydberg state predissociation dynamics depend on the rotational transition. At the same time, the angular distributions of the products can aid in determining the spectral assignments, as discussed above. Our principal observation is that the angular distributions vary strongly with rotational transition in a manner that is predicted by Eq. (5). Since this equation involves a coherent sum over possible intermediate states, and since the resulting angular distributions are very sensitive to the mixture of intermediate states, measurement of the angular distributions also provides a method for assessing the relative contributions of the intermediate states.

The experimental spectra in the three Rydberg regions we investigated consist mainly of blended lines, where progressions such as $Q_{21}+R_{11}$ cannot be resolved. The situation is even more complicated in the $6d\pi^-(v=1)/5s\sigma(v=3)$ region where there is overlap between branches from the two electronic transitions. The spectral assignment discussed above identifies the contributions to each of the peaks in the Rydberg regions. The two-photon line strengths, calculated by integrating the results of Eq. (5) over angle, were compared to the line intensities and allowed calculation of the rotational temperature of the expansion, so that we are able to quantify each contribution to lines that were overlapped. The theoretical angular distributions are therefore calculated by using the different rotational and electronic contributions weighted by the corresponding Boltzmann factor and the line strengths involved. In cases where lines from the transition to the $6d\pi^-(v=1)$ overlap with lines corresponding to the $5s\sigma(v=3)$ transition, we made the assumption that the two transitions have equal transition moments. Our experimental angular distributions are consistent with this assumption. Table II gives both the experimentally and theoretically obtained β and γ values, where the theoretical values were calculated by fitting the result of Eq. (5) with the formula $I(\theta)\propto 1+\beta P_2(\cos\theta)+\gamma P_4(\cos\theta)$. Samples of the experimental and theoretical angular distributions are given in Fig. 6.

In the $8d\pi^-(v=1)$ Rydberg region, the $Q_{21}+R_{11}$ and the $Q_{11}+P_{21}$ are the dominant progressions. However the $Q_{21}+R_{11}(J=2.5)$ transition overlaps with the $S_{11}+R_{21}(J=2.5)$ line, and therefore the angular distribution is a contribution from both of these transitions. The peak corresponding to the $Q_{11}+P_{21}$ transition is made up of three different lines in the progression for $J=1.5$, 2.5, and 3.5. The theoretical angular distributions agree well with the experimental ones for all the transitions imaged, except for the $Q_{21}+R_{11}(J=0.5)$ line.

The $5s\sigma(v=2)$ Rydberg transition is only 0.04 eV above the threshold for channel (6). The small amount of excess energy and the weak predissociation of some of the rotational transitions makes imaging of these lines quite challenging. The noise in the experimental angular distributions is therefore much higher in this region. Nonetheless, the experimental angular distributions again agree well with the theoretical ones, except for the $P_{11}(J=1.5)$ line.

The $6d\pi^-(v=1)/5s\sigma(v=3)$ region is complicated by the mixing of the two electronic transitions. One of the tools used in assigning this region is the comparison between the theoretical and experimental angular distributions. Based on this comparison, we are able to distinguish between the rotational lines corresponding to either the π or the σ transition. The contributions involved in each of the peaks present in the $6d\pi^-(v=1)/5s\sigma(v=3)$ spectrum are described in Table II. We find reasonable agreement between the experi-

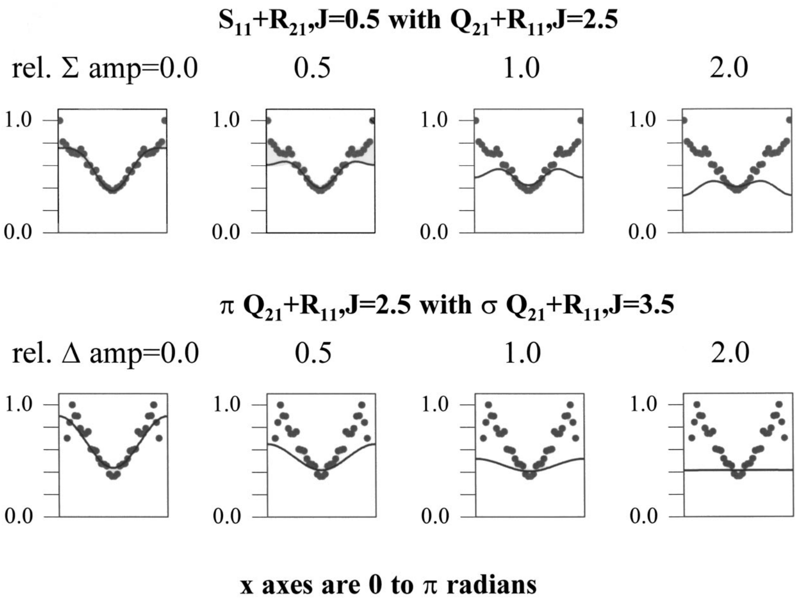

FIG. 7. Angular data for transitions in the $8d\pi^-$ $(v=1)$ (top) and the $6d\pi^-$ $(v=1)/5s\sigma$ $(v=3)$ (bottom) region and the theoretical fits obtained assuming various relative amplitudes for either Σ (upper panels) or Δ (lower panels) intermediates. The amplitude of the Π intermediate is maintained at unity.

ment and theory, except again for the $P_{11}(J=1.5)$ and also the $Q_{11}+P_{21}(J=1.5)$, both belonging to the σ transition. We note that the $Q_{21}+R_{11}(J=0.5)$ line belonging to the $6d\pi^-$ transition is overlapped with the $Q_{21}+R_{11}(J=1.5)$ belonging to the $5s\sigma$ state. If only the Boltzmann factors and the line strengths are considered, then the angular distribution for this peak would be dominated by the $Q_{21}+R_{11}(J=0.5)$ line of the $6d\pi^-$ transition and would not agree well with the theoretically predicted distribution. However, as noted in the discussion of the spectral assignments, the experimental spectra reveal that the $5s\sigma(v=3)$ transition is much more strongly predissociative than the $6d\pi^-(v=1)$ transition. If this factor is taken into account, and the theoretical angular distribution is obtained by giving the majority of the contribution (70%) to the transition involving the $5s\sigma(v=3)$ state, then we obtain a good agreement with the experimental angular distribution.

Although the majority of the data agree reasonably with the theoretical predictions, we note that the angular distributions for the $P_{11}(J=1.5)$ and $Q_{11}+P_{21}(J=1.5)$ lines of the $5s\sigma(v=3)$ level, the $P_{11}(J=1.5)$ line of the $5s\sigma(v=2)$ level, and the $Q_{21}+R_{11}(J=0.5)$ line of the $8d\pi^-(v=1)$ level are inconsistent with the theoretical prediction. These lines all terminate in $J=0.5$ levels. Because there are only two m_J levels, either $+\frac{1}{2}$ or $-\frac{1}{2}$, and because linear polarization cannot create a difference in population between these (regardless of the symmetry of the two-photon intermediate state), we must create an isotropic spatial distribution in $J=0.5$. This isotropic distribution is also predicted by Eq. (5). However, the data for the lines listed above nearly always indicates more population at 0 and π radians, the north and south poles, than at the $\pi/2$ radians, the equator. We investigated two experimental possibilities for the deviation. First, it is possible that the $O(^3P_2)$ is created with a laboratory alignment, such as is the case, for example, in the dissociation of NO_2.[39,40] However, the angular distributions measured on several of these transitions did not change when the polarization of the probe laser was changed from vertical to horizontal while holding the polarization of the pump laser in the vertical direction. Nor was there any difference between the angular distribution obtained for $O(^3P_2)$ and that obtained for $O(^3P_0)$, where no such alignment can occur. We conclude that the oxygen atom products are not aligned. We also checked to see whether a small degree of elliptical polarization could change the angular distributions significantly; it did not. We thus believe that the data are accurate and that the theory, while not in agreement with the data, is correct. The only way out of this dilemma that we can see involves either a process that affects the final, $J=0.5$, levels or the intermediate levels, the $J=1.5$ levels of the $C\,^2\Pi$ state (see discussion below). It is hard to see how some process operating on the final level, for example differential depletion of m_J levels by ionization, could make such a profound change in the angular distribution, especially since the lasers are linearly polarized and thus must operate equally on $m_J=\pm\frac{1}{2}$. On the other hand, it is known that there is strong mixing between low rotational levels of the $C\,^2\Pi$ Rydberg state and the $B\,^2\Pi$ valence state.[3,41] It is conceivable, though admittedly not likely, that this perturbation provides amplitude to a rotationally broadened Rydberg state that has a parallel component.

The theoretical angular distributions predicted by Eq. (5) depend strongly on the mixture of intermediate states in the two-photon transition. In fitting the $8d\pi^-$ level, Pratt *et al.* assumed equal amplitudes of case (b) Π and Σ intermediates. We find this ratio not to agree with the angular data, which indicates that the Σ state must make a minor or negligible contribution. In all of the angular fits shown in Fig. 6 or listed in Table II, we have assumed that the intermediate is of Π symmetry. Figure 7 shows angular data for two specific transitions, both in the $6d\pi^-(v=1)/5s\sigma(v=3)$ region, and the fits to the data assuming various amplitudes for either Σ (upper panels) or Δ (lower panels) intermediates. The amplitude of the Π intermediate is taken to be unity, while the predicted angular distributions for the data are shown for relative amplitudes of 0, 0.5, 1.0, and 2.0 for either Σ or Δ

intermediates. It is clear from the figure that the best fit is for the relative amplitude of either the Σ or Δ state to be zero. We note that the sensitivity of the angular distribution to these relative amplitudes provides an excellent experimental method for determining the contributions from intermediate states of differing symmetry.

VI. CONCLUSIONS

Product imaging has been found in this work to be an extremely valuable tool in assigning and understanding the two-photon excitation spectra and dynamics of NO Rydberg levels. Rotational assignments can be checked by comparing the angular distributions predicted by Eq. (5) with those measured on rotationally resolved lines. They may also be used to identify the contributions of various intermediate states to the two-photon line strength. By use of these techniques, we have assigned the spectra in the $6d\pi^-(v=1)/5s\sigma(v=3)$ region and have reinterpreted the spectra previously described by Umemoto and Matsumoto.[23] The major contribution to the two-photon excitation process for all the Rydberg levels we investigated comes from an intermediate of Π symmetry, likely the $C\,^2\Pi$ state. The atomic products are predominantly $\mathrm{N}(^2D)+\mathrm{O}(^3P)$.

ACKNOWLEDGMENTS

This work was supported by The Department of Energy under Grant No. DE-FG02-88ER13934 and, in part, by the National Science Foundation, under Grant No. CHE-9901065. The authors gratefully acknowledge the assistance of Nate Emmott and Indira Gopal, and we appreciate having received spectral data from Dr. Stephen Pratt.

[1] E. Miescher and F. Alberti, J. Phys. Chem. Ref. Data **5**, 309 (1976).
[2] E. Miescher and K. P. Huber, Int. Rev. Sci. Phys. Chem. (Series 2) **3**, 37 (1976).
[3] S. Fredin, D. Gauyacq, M. Horani, C. Jungen, and G. Lefevre, Mol. Phys. **60**, 825 (1987).
[4] P. M. Johnson, M. R. Berman, and D. Zakheim, J. Chem. Phys. **62**, 2500 (1975).
[5] D. Zakheim and P. Johnson, J. Chem. Phys. **68**, 3644 (1978).
[6] M. G. White, W. A. Chupka, M. Seaver, A. Woodward, and S. D. Colson, J. Chem. Phys. **80**, 678 (1984).
[7] F. Lahmani, C. Lardeaux, D. Solgadi, A. Zehnacker, I. Dimicoli, M. Boivineau, M. Mons, and F. Piuzzi, J. Phys. Chem. **89**, 5646 (1985).
[8] S. T. Pratt, Chem. Phys. Lett. **151**, 138 (1988).
[9] E. R. Sirkin, M. Asscher, and Y. Haas, Chem. Phys. Lett. **86**, 265 (1982).
[10] R. G. Bray, R. M. Hochstrasser, and J. E. Wessel, Chem. Phys. Lett. **27**, 167 (1974).
[11] J. C. Miller and R. N. Compton, Chem. Phys. Lett. **93**, 453 (1982).
[12] K. S. Viswanathan, E. Sekreta, E. R. Davidson, and J. P. Reilly, J. Phys. Chem. **90**, 5078 (1986).
[13] J. C. Miller and R. N. Compton, J. Chem. Phys. **75**, 22 (1981).
[14] J. C. Miller and R. N. Compton, J. Chem. Phys. **84**, 675 (1986).
[15] Y. Achiba, K. Sato, and K. Kimura, J. Chem. Phys. **82**, 3959 (1985).
[16] K. Tsukuyama, T. Munakata, M. Tsukakoshi, and T. Kasuya, Chem. Phys. Lett. **137**, 315 (1987).
[17] D. Gauyacq, S. Fredin, and Ch. Jungen, Chem. Phys. **117**, 457 (1987).
[18] S. T. Pratt, Ch. Jungen, and E. Miescher, J. Chem. Phys. **90**, 5971 (1989).
[19] R. G. Bray and R. M. Hochstrasser, Mol. Phys. **31**, 1199 (1976).
[20] J. B. Halpern, H. Zacharias, and R. Wallenstein, J. Mol. Spectrosc. **79**, 1 (1980).
[21] L. E. Jusinski, G. E. Gadd, G. Black, and T. G. Slanger, J. Chem. Phys. **90**, 4282 (1989).
[22] G. E. Gadd, L. E. Jusinski, and T. G. Slanger, J. Chem. Phys. **91**, 3378 (1989).
[23] H. Umemoto and K. Matsumoto, J. Chem. Soc., Faraday Trans. **92**, 1315 (1996).
[24] A. Fujii and N. Morita, Laser Chem. **13**, 259 (1993).
[25] B. L. G. Bakker, A. T. J. B. Eppink, D. H. Parker, M. L. Costen, G. Hancock, and G. A. D. Ritchie, Chem. Phys. Lett. **283**, 319 (1998).
[26] B. L. G. Bakker, D. H. Parker, G. Hancock, and G. A. D. Ritchie, Chem. Phys. Lett. **294**, 565 (1998).
[27] R. J. Wilson, J. A. Mueller, and P. L. Houston, J. Phys. Chem. A **101**, 7593 (1997).
[28] B.-Y. Chang, R. C. Hoetzlein, J. A. Mueller, J. D. Geiser, and P. L. Houston, Rev. Sci. Instrum. **69**, 1665 (1998).
[29] D. J. Bamford, L. E. Jusinski, and W. K. Bischel, Phys. Rev. A **34**, 185 (1986).
[30] D. J. Bamford, M. J. Dyer, and W. K. Bischel, Phys. Rev. A **36**, 3497 (1987).
[31] H. Umemoto, M. Kashiwazaki, and T. Yahata, J. Chem. Soc., Faraday Trans. **94**, 1793 (1998).
[32] A. T. J. B. P. Eppink and D. H. Parker, Rev. Sci. Instrum. **68**, 3477 (1997).
[33] NIST Atomic Spectra Database; Version 2.0; NIST Standard Reference Database #78; http://physics.nist.gov/cgi-bin/AtData/main_asd
[34] P. C. Cross, R. M. Hainer, and G. W. King, J. Chem. Phys. **12**, 210 (1944).
[35] R. N. Zare, *Angular Momentum* (Wiley, New York, 1988).
[36] K. P. Huber and G. Herzberg, *Molecular Spectra and Molecular Structure IV. Constants of Diatomic Molecules* (Van Nostrand Reinhold, New York, 1979).
[37] L. L. A. East, J. Chem. Phys. **109**, 2185 (1998).
[38] B. Urban, A. Strobel, and E. V. Bondybey, J. Chem. Phys. **111**, 8939 (1999).
[39] M. Ahmed, D. S. Peterka, and A. G. Suits, in *Advances in atomic and molecular research and applications*, edited by R. Compargue (Springer, Berlin, 2001), p. 343.
[40] E. R. Wouters, M. Ahmed, D. S. Peterka, A. S. Bracker, A. G. Suits, and O. S. Vasyutinskii, ACS Symp. Ser. **770**, 238 (2000).
[41] E. Miescher, J. Mol. Spectrosc. **53**, 302 (1974).